


## RESEARCH ARTICLE

# Nanoscale imaging of pT217-tau in aged rhesus macaque entorhinal and dorsolateral prefrontal cortex: Evidence of interneuronal trafficking and early-stage neurodegeneration

Dibyadeep Datta<sup>1,2</sup>  | Isabella Perone<sup>1</sup> | Denethi Wijegunawardana<sup>1</sup> | Feng Liang<sup>3</sup> | Yury M. Morozov<sup>1</sup> | Jon Arellano<sup>1</sup> | Alvaro Duque<sup>1</sup> | Zhongcong Xie<sup>3</sup> | Christopher H. van Dyck<sup>2</sup> | Mary Kate P. Joyce<sup>1</sup> | Amy F. T. Arnsten<sup>1</sup>

<sup>1</sup>Department of Neuroscience, Yale University, School of Medicine, New Haven, Connecticut, USA

<sup>2</sup>Department of Psychiatry, Yale University, School of Medicine, New Haven, Connecticut, USA

<sup>3</sup>Department of Anesthesia, Critical Care and Pain Medicine, Massachusetts General Hospital and Harvard Medical School, Boston, Massachusetts, USA

## Correspondence

Amy F. T. Arnsten, Albert E. Kent Professor of Neuroscience, Department of Neuroscience, Yale Medical School, 333 Cedar St., New Haven, CT 06510, USA.  
Email: [amy.arnsten@yale.edu](mailto:amy.arnsten@yale.edu)

Dibyadeep Datta, Department of Psychiatry, Yale School of Medicine, 333 Cedar St. New Haven, CT 06510, USA.  
Email: [dibyadeep.datta@yale.edu](mailto:dibyadeep.datta@yale.edu)

## Funding information

National Institutes of Health (NIH), Grant/Award Numbers: AG079145-01, AG061190-01; American Federation for Aging Research (AFAR) Faculty Transition; Yale Alzheimer's Disease Research Center, Grant/Award Number: P30AG066508; Pilot Project and Research Scholar; MacBrain Resource Center, Grant/Award Number: MH113257; Anesthesia Biomarker Core at Massachusetts General Hospital, Grant/Award Number: R01 AG RF1AG070761

## Abstract

**INTRODUCTION:** Tau phosphorylated at threonine-217 (pT217-tau) is a novel fluid-based biomarker that predicts onset of Alzheimer's disease (AD) symptoms, but little is known about how pT217-tau arises in the brain, as soluble pT217-tau is dephosphorylated *post mortem* in humans.

**METHODS:** We used multilabel immunofluorescence and immunoelectron microscopy to examine the subcellular localization of early-stage pT217-tau in entorhinal and prefrontal cortices of aged macaques with naturally occurring tau pathology and assayed pT217-tau levels in plasma.

**RESULTS:** pT217-tau was aggregated on microtubules within dendrites exhibiting early signs of degeneration, including autophagic vacuoles. It was also seen trafficking between excitatory neurons within synapses on spines, where it was exposed to the extracellular space, and thus accessible to cerebrospinal fluid (CSF)/blood. Plasma pT217-tau levels increased across the age span and thus can serve as a biomarker in macaques.

**DISCUSSION:** These data help to explain why pT217-tau predicts degeneration in AD and how it gains access to CSF and plasma to serve as a fluid biomarker.

## KEYWORDS

biomarker, dorsolateral prefrontal cortex, entorhinal cortex, plasma, tau phosphorylated at threonine-217, trafficking

This is an open access article under the terms of the [Creative Commons Attribution](https://creativecommons.org/licenses/by/4.0/) License, which permits use, distribution and reproduction in any medium, provided the original work is properly cited.

© 2024 The Authors. *Alzheimer's & Dementia* published by Wiley Periodicals LLC on behalf of Alzheimer's Association.

## 1 | BACKGROUND

Recent advances in Alzheimer's disease (AD) research have revealed a novel fluid-based biomarker, tau phosphorylated at threonine-217 (pT217-tau), in cerebrospinal fluid (CSF) and blood plasma, that reliably discriminates AD from other neurodegenerative diseases.<sup>1</sup> pT217-tau appears in the earliest presymptomatic stages of AD<sup>1,2</sup> and predicts subsequent cognitive decline.<sup>3</sup> Moreover, plasma pT217-tau—among multiple tau species and other biomarkers—has demonstrated the highest accuracy to predict the presence of AD neuropathology, including aggregated tau pathology.<sup>4</sup> Novel diagnostic biomarkers will be critical for assessing efficacy of novel therapeutic treatments aimed at early-stage disease.<sup>5,6</sup> However, it is unknown why this specific phosphorylated tau species is so effective in predicting brain pathology, as little is known about early, soluble pT217-tau expression in the brain. It is especially challenging to address this issue in the human brain, as soluble phosphorylated tau is rapidly dephosphorylated *post mortem*, and positron emission tomography (PET) scans detect late-stage, fibrillated tau but not the earlier-stage, soluble pT217-tau that likely gives rise to the signal in CSF and plasma.<sup>7</sup> However, the etiology of pT217-tau in the aging brain can be addressed in rhesus macaques, where perfusion fixation allows capture of phosphorylated proteins in their native state.<sup>8</sup>

Aging rhesus macaques naturally develop tau pathology with the same qualitative pattern and sequence as humans, including initial cortical pathology in layer II of the entorhinal cortex (ERC), and later in layer III of the dorsolateral prefrontal cortex (dlPFC).<sup>8</sup> As with humans, tau pathology begins in dendrites of excitatory neurons, where tau hyperphosphorylation leads to aggregation and subsequent fibrillation, forming neurofibrillary tangles within neurons that die via autophagic degeneration.<sup>9,10</sup> Neuropathological studies show that tau pathology begins about a decade prior to formation of amyloid beta (A $\beta$ ) plaques,<sup>11</sup> and correlates with gray matter loss<sup>12</sup> and cognitive impairment.<sup>13</sup> Recent evidence indicates that phosphorylated tau can spread by “seeding” between interconnected neurons, with the ERC a likely origin early in disease,<sup>10,14–17</sup> a finding that has been replicated in rodent AD models.<sup>17–25</sup> However, little is known about the etiology of pT217-tau in the human brain, as both *post mortem* and PET imaging studies can only capture fibrillated tau, which occurs at a much later stage. Perfusion fixation of monkey tissue preserves not only phosphorylation state, but internal membranes and organelle architecture, and thus allows high-resolution imaging of molecular location and interactions with cellular organelles at the ultrastructural level, including the detection of large, autophagic vacuoles as early indicators of neurodegeneration.

The current study examined the expression pattern of pT217-tau in aged macaque ERC and dlPFC, including whether pT217-tau could be seen within neurons with early signs of autophagic degeneration, consistent with its predicting future neurodegeneration and disease. We also used high magnification immuno-electron microscopy (immunoEM) to determine whether there was evidence of pT217-tau trafficking between neurons to “seed” tau pathology in higher brain circuits, interfacing with the extracellular space to become accessible to

### RESEARCH IN CONTEXT

- 1. Systematic review:** Tau phosphorylated at threonine-217 (pT217-tau) is a novel fluid-based biomarker that heralds the onset of Alzheimer's disease (AD) symptoms. However, little is known about its pathogenesis in the brain, as soluble pT217-tau is lost *post mortem* in humans.
- 2. Interpretation:** The current study of pT217-tau expression in perfusion-fixed aged macaque cortex shows that pT217-tau aggregates in dendrites undergoing the early stages of degeneration and thus serves as an index of the neurodegenerative process. We also report the first evidence of soluble, pT217-tau undergoing transsynaptic trafficking between neurons to “seed” tau pathology in higher brain circuits, where it interfaces with the extracellular space and becomes accessible to cerebrospinal fluid and blood. pT217-tau levels also increase with age in macaque plasma.
- 3. Future directions:** Future research can use plasma and cortical pT217-tau levels in aging macaques to assess the efficacy of potential treatments, especially those aimed at inhibiting early-stage pathology.

CSF/blood as a fluid biomarker. As immunoEM requires in-depth focus, we examined two cortical areas vulnerable to tau pathology: layer II ERC where cortical pathology first begins, and layer III dlPFC, where tau pathology emerges later. We selected age ranges when pT217-tau would be expressed, but still soluble, and thus able to traffic between neurons, and when we first see signs of autophagic degeneration: that is, 18 to 24 years for ERC and 26 to 31 years for dlPFC. We also examined pT217-tau in plasma from rhesus macaques across the entire extent of the macaque age span (1–34 years), to determine whether it increases with age and can serve as a fluid biomarker in macaques as well as humans. The data revealed that pT217-tau has extensive accumulation within layer II ERC and layer III dlPFC excitatory neurons that express early signs of autophagic degeneration and can be seen trafficking between neurons where it is exposed to the extracellular space, helping to explain why it is an effective, fluid biomarker of early degenerative events in brain.

## 2 | METHODS

### 2.1 | Electron microscopy

#### 2.1.1 | Animals and tissue processing

Three “early” aged (18–24 years) and five “late” aged (26–31 years) rhesus monkeys (*Macaca mulatta*) were used in this study and were maintained and euthanized in accordance with the guidelines



of the US Department of Agriculture, the Yale University Institutional Animal Care and Use Committee (IACUC), and in accordance with the Weatherall report. As described previously,<sup>26-29</sup> primates were deeply anesthetized prior to transcatheter perfusion of 100 mM phosphate-buffered saline, followed by 4% paraformaldehyde/0.05% glutaraldehyde in 100 mM phosphate-buffered saline. After perfusion, a craniotomy was performed, and the entire brain was removed and blocked. The brains were sectioned coronally at 60  $\mu$ m on a vibratome (Leica) across the entire rostrocaudal extent of the ERC and dlPFC (Walker's area 46). The sections were cryoprotected through increasing concentrations of sucrose solution (10%, 20%, and 30% each for overnight), cooled rapidly using liquid nitrogen, and stored at  $-80^{\circ}\text{C}$ . Sections of ERC and dlPFC were processed for immunocytochemistry. To enable penetration of immunoreagents, all sections went through three freeze-thaw cycles in liquid nitrogen. Non-specific reactivity was suppressed with 10% normal goat serum (NGS) and 5% bovine serum albumin (BSA), and antibody penetration was enhanced with 0.3% Triton X-100 in 50 mM Tris-buffered saline (TBS).

## 2.1.2 | Histology and immunoreagents

Previously characterized primary antibodies for pT217-tau raised in rabbits were used, and complexed with species-specific goat secondary antibodies. The following primary antibodies were used: (1) rabbit anti-pT217-tau at 1:200 (cat# AS-54968, Anaspec). The immunogen used keyhole limpet hemocyanin conjugated with synthetic peptides corresponding to human tau at phosphorylated threonine 217; (2) rabbit anti-pT217-tau at 1:200 (cat # 44-744, Thermo Fisher). The antiserum was produced against a chemically synthesized phosphopeptide derived from the region of human tau that contains threonine 217. Both primary antibodies for pT217-tau produced comparable results; (3) mouse anti-EEA1 at 1:250 (cat# 610456, BD Biosciences); (4) mouse anti-Amyloid- $\beta$ 1-42 IgG2b (clone MOAB-2) at 1:300 (cat# NBP213075, Novus). This antibody recognizes unaggregated, oligomeric, and fibrillary forms of A $\beta$ 42 and unaggregated A $\beta$ 40, and has been previously used in aged macaque tissue to characterize Braak stage III/IV AD-like pathology;<sup>8</sup> (5) mouse antiphosphoSer202/Thr205-tau IgG1k (clone AT8) at 1:300 (cat# MN1020; Thermo Fisher Scientific); (6) mouse monoclonal casein kinase I $\delta$  Antibody (cat #sc-55553, Santa Cruz Biotechnology); (7) goat polyclonal casein kinase I $\delta$  Antibody (cat #NB100-2919; Novus Biologicals). The specificity and selectivity of the primary antibodies have been characterized using immunoblot, immunohistochemistry, immunofluorescence, and enzyme-linked immunosorbent assay approaches in various tissue types in multiple species.<sup>30-35</sup> Normal sera and immunoglobulin G (IgG)-free BSA were purchased from Jackson ImmunoResearch. All chemicals and supplies for electron microscopy were purchased from Sigma Aldrich and Electron Microscopy Sciences, respectively.

## 2.1.3 | Single pre-embedding peroxidase immunocytochemistry

As described previously,<sup>26</sup> the sections were incubated for 72 hours at  $4^{\circ}\text{C}$  with primary antibodies in TBS, and transferred for 2 hours at room temperature to species-specific biotinylated Fab' or F(ab')<sub>2</sub> fragments in TBS. To reveal immunoperoxidase labeling, sections were incubated with the avidin-biotin peroxidase complex (ABC; 1:300; Vector Laboratories) and then visualized in 0.025% Ni-intensified 3,3-diaminobenzidine tetrahydrochloride (DAB; Sigma Aldrich) as a chromogen in 100 mM phosphate buffer (PB) with the addition of 0.005% hydrogen peroxide for 8 minutes. After the DAB reaction, sections were exposed to osmification (concentration 1%), dehydration through a series of increasing ethanol concentrations (70%-100%), and infiltrated with propylene oxide. Tissue sections were counterstained with 1% uranyl acetate in 70% ethanol. Standard epoxy resin embedding followed typical immunoEM procedures followed by polymerization at  $60^{\circ}\text{C}$  for 60 hours. Omission of primary antibodies or substitution with non-immune serum resulted in complete lack of immunoperoxidase labeling. Similarly, labeling was nullified when blocking the biotinylated probes with avidin/biotin.

## 2.1.4 | Double-label pre-embedding gold and peroxidase immunohistochemistry

Double-label immunoEM was accomplished by pairing gold (for A $\beta$ ) and DAB (for pT217-tau) in dlPFC of two "late-aged" female macaques, aged 24 and 26 years. Sections underwent a 50 mM glycine in 0.1 M PBS incubation for 1 hour (Sigma, cat# G-7126), a 30 minute 0.3% hydrogen peroxide incubation at  $4^{\circ}\text{C}$ , and avidin-biotin blocking (Vector cat# SP-2001) to prevent non-specific labeling from free aldehydes, and the immunoperoxidase product, respectively. Sections were blocked for 1 hour at room temperature (RT; 5% BSA, 10% NGS, 0.4% Triton X-100, and 0.1% Aurion acetylated BSA, or BSA-c, Electron Microscopy Sciences, cat# 25557, in 0.1 M PB), and incubated in Anaspec rabbit anti-pT217-tau at 1:200 for 72 hours at  $4^{\circ}\text{C}$ . After removal from the primary antibody incubation, sections were incubated in biotinylated F(ab')<sub>2</sub> fragment goat anti-rabbit at 1:200 (Jackson ImmunoResearch cat# 111-066-144) for 3 hours at RT, and then underwent avidin-biotin amplification using ABC, as above, and were visualized using a DAB kit (Vector SK-4100) with no nickel intensification for 3 minutes. Then, sections were incubated in the mouse anti-Amyloid- $\beta$ 1-42 at 1:300 for 72 hours at  $4^{\circ}\text{C}$ . After removal from the primary antibody, sections were incubated in Aurion F(ab) fragment of goat anti-mouse ultrasmall at 1:50 (Electron Microscopy Sciences, cat#25415) for 3 hours at RT. Subsequently, sections underwent a 4% paraformaldehyde (in PBS) postfix for 5 minutes, followed by a 10 minute 50 mM glycine incubation to quench free aldehydes, and a few quick distilled water washes. Silver enhancement was performed with the Nanoprobes HQ Silver kit (cat# 2012-45ML) in the dark for 20 to 30 minutes, and produced variable-sized particles.

Sections were first post-fixed in 4% paraformaldehyde in 0.1 M PBS for 20 minutes, then were submerged in 1% osmium tetroxide in PB, followed by immediate dilution by half (to 0.5%), and the sections incubated in the dark for 30 minutes at 4°C. Sections then proceeded with the remainder of EM processing steps as described in the preceding section.

### 2.1.5 | Electron microscopy and data analysis

For single-label immunoperoxidase immunohistochemistry, sections were mounted on microscope slides and ERC layer II and dIPFC layer III were photographed under an Olympus BX51 microscope equipped with a Zeiss AxioCam charge-coupled device camera. Zeiss AxioVision imaging software was used for imaging and data acquisition. All sections were processed as previously described and immunoEM imaging was conducted in ERC layer II and dIPFC layer III.<sup>26</sup> Briefly, blocks containing ERC layer II and dIPFC layer III were sampled and mounted on resin blocks. The specimens were cut into 50 nm sections using an ultramicrotome (Leica) and analyzed under a Talos L120C transmission electron microscope (Thermo Fisher Scientific). Several plastic blocks of each brain were examined using the 4th to 12th surface-most sections of each block (i.e., 200–600 nm), to sample the superficial component of sections, avoiding penetration artifacts. Structures were digitally captured at  $\times 25,000$  to  $\times 100,000$  magnification with a Ceta complementary metal oxide semiconductor (CMOS) camera and individual panels were adjusted for brightness and contrast using Adobe Photoshop and Illustrator CC.2020.01 image editing software (Adobe Systems Inc.). Approximately 5000 micrographs of selected areas of neuropil with immunopositive profiles were used for analyses with well-defined criteria.

For profile identification, we adopted the criteria summarized in Peters et al.<sup>36</sup> Dendritic spines in the prefrontal cortex are typically long and thin, devoid of mitochondria, with the presence of a noticeable postsynaptic density (PSD) at asymmetric synapses, and often containing an elaborated spine apparatus, the extension of the smooth endoplasmic reticulum into the spine. Dendritic shafts were typically round in perpendicular planes or irregular shaped when assessed in horizontal planes, usually containing mitochondria and numerous tubular and pleomorphic cellular organelles. Depending on the proximity to axon terminals, various dendritic shafts received synaptic inputs. Axon terminals contained accumulations of synaptic vesicles and the axoplasm of these terminals usually contained neurofilaments and mitochondria. The synaptic innervations made by these axon terminals were either asymmetric, containing spherical vesicles, or symmetric, containing pleomorphic vesicles, with typical differences in PSD, respectively. Unmyelinated axons were small, round processes with a predominantly even and regular shape, traversing the neuropil in a straight orientation, often forming bundles in perpendicular planes. Astrocytic processes were typically of irregular morphology, forming contours that filled the empty space around neuronal elements.

To evaluate whether there was concordance between dendrites immunopositive for pT217-tau and signatures of autophagic degen-

eration, quantitative assessments were performed on a series of low and high magnification 2D micrographs of ERC layer II and supra-granular dIPFC layer III. Each field covered an area of 15 to 30  $\mu\text{m}^2$  captured from the thin sections in early-aged ERC and late-aged dIPFC in rhesus macaques for analyses. Approximately 200 micrographs of selected areas of neuropil with immunopositive profiles were used for quantitative analyses. Autophagic vacuoles were identified based on multilamellar bodies, containing partially degraded cytoplasmic materials. The frequency of pT217-tau positive elements was highly consistent across all animals and pooled across animals within an age group.

### 2.2 | Immunofluorescence with confocal microscopy

Immunofluorescence staining was carried out on free-floating sections as described previously.<sup>37</sup> Three adult (8–10 years), two “early” aged (18–19 years), and four “late” aged (28–34 years) rhesus monkeys (*Macaca mulatta*) were used in this study. Antigen retrieval was performed with 10 mM solution citrate buffer in a hot water bath for 25 minutes at high temperature. The free-floating sections were left to cool for 30 minutes at RT. The sections were transferred to 1X TBS for 10 minutes. Sections were then incubated in 0.5% sodium borohydride in 0.01 M TBS. Sections were blocked for 1 hour at RT in 1X TBS containing 5% BSA, 2% Triton X-100, and 10% normal goat serum. Sections were incubated for 72 hours at 4°C with pT217-tau primary antibody (dilution 1:100; see supplier information above), MAP2 (dilution 1:1000; ab5392, Abcam), mouse antiphosphoSer202/Thr205-tau IgG1k (clone AT8; dilution 1:300; cat# MN1020; Thermo Fisher Scientific), casein kinase I $\delta$  antibody (dilution 1:100; cat #sc-55553, Santa Cruz Biotechnology), goat polyclonal casein kinase I $\delta$  antibody (dilution 1:100; cat #NB100-2919; Novus Biologicals), followed by incubation overnight at 4°C with secondary antibodies (1:1000, Alexa-Fluor conjugated, Invitrogen). After incubation in secondary antibodies, they were incubated in 70% ethanol with 0.3% Sudan Black B (MP Biomedicals, cat# 4197-25-5), to decrease autofluorescence from lipofuscin, and counterstained with Hoechst (1:10,000, Thermo Fisher, cat# H3570). The sections were mounted in ProLong Gold Antifade Mountant (Invitrogen, cat# P36930). Confocal images from ERC layer II and dIPFC layer III were acquired using a Zeiss LSM 880 Airyscan Confocal Microscope, with the C-Apochromat 40x/1.2 W Korr FCS M27 (Zeiss) water objective. Emission filter bandwidths and sequential scanning acquisition were set up to avoid possible spectral overlaps between fluorophores. Images were merged using Fiji software.

### 2.3 | Measurement of pT217-tau in blood plasma by nanoneedles

Fifteen young (1–17 years) and twenty-one aged (18–34 years) rhesus monkeys (*Macaca mulatta*) were used in the plasma pT217-tau

study (total cohort  $N = 36$ ). Blood plasma was collected during routine tuberculosis testing for rhesus macaques. We developed in-house phosphorylated tau assays using the nanoneedle technology to measure plasma concentrations of pT217-tau. More than 20,000 nanoneedles are integrated on a silicon substrate assigned to detect one analyte. Each nanoneedle is a single-molecule biosensor functionalized with antibodies. Because phosphorylated tau in blood samples is present at low abundance, the binding events of phosphorylated tau on the nanoneedle sensor array follow Poisson statistics, that is, one or no molecule is captured on each nanoneedle. This allows precise quantitation of analytes by digitally counting the number of nanoneedles that have a positive signal. In the present study, we developed sandwich-type pT217-tau assays to measure the ultra-low concentration of protein levels in patient blood samples. The nanoneedle chip was provided by NanoMosaic. Nanoneedles are fabricated in an array format with a spacing of 1.8  $\mu\text{m}$ . Each nanoneedle has a diameter of  $< 100$  nm. The nanoneedle surfaces were modified with 0.5% 3-aminopropyltrimethoxysilane (APTMS) and activated with 2% glutaraldehyde. This enables antibodies to covalently bind on the surface of the nanoneedles.<sup>38</sup> We used 5  $\mu\text{g}/\text{ml}$  capture antibody concentration and incubated with chip overnight. We then washed the chip in PBS and incubated it with blocking solution for 1 hour. Five  $\mu\text{l}$  of plasma samples were thawed and diluted 2 X into the dilution buffer provided by NanoMosaic. The diluted sample was incubated on the chip for 2 hours. After washing, a biotinylated detection antibody at 0.5  $\mu\text{g}/\text{ml}$  was incubated on the chip. Next, 0.5  $\mu\text{g}/\text{ml}$  streptavidin-horseradish peroxidase (HRP) conjugate was incubated for 30 minutes, and 3,3',5,5'-tetramethylbenzidine (TMB) provided by NanoMosaic was applied on the chip for 15 minutes to illuminate the HRP. The enzymatic reaction produced a non-soluble precipitate on the nanoneedles when the sandwich complex was present. The precipitate changes the local refractive index of the nanoneedle and induces a color shift intrinsic to the nanoneedle property. The nanoneedles are imaged under a dark-field configuration with a CMOS color camera before and after the assay using the Tessie™ instrument from NanoMosaic. Software provided by NanoMosaic analyzed the colors of all nanoneedles and reported the percentage of the color-shifted number of nanoneedles. We used phospho-specific antibodies to pT217-tau (Thermo Fisher 44-744) as the detection antibodies for pT217-tau measurement. The specificity of the phospho-specific antibodies to pT217-tau was validated with peptide array, described in the following section.

The protein levels are reported in relative units specific to the nanoneedle technology (i.e., Nano Unit) as described in previous studies<sup>39,40</sup> because pT217-tau recombinant protein standards are not available at present. All measurement results were above the lower limit of detection of the nanoneedle assay. Assay specificity was validated with dot blot measurement of the phospho-specific antibodies against an array of synthesized peptides phosphorylated at different residues along the full-length tau protein as described in a previous study.<sup>39</sup>

## 2.4 | Statistical analysis of rhesus macaque blood plasma pT217-tau data

To assess age-related alterations in pT217-tau expression in blood plasma during age span, a Pearson's correlation regression analysis was computed. For group analysis, a Welch  $t$  test was performed because the pT217-tau expression in blood plasma was normally distributed. Fits were modelled as linear and exponential growth equations.

## 3 | RESULTS

### 3.1 | Aged rhesus monkeys show progressive development of pT217-tau immunolabeling

Our previous research has demonstrated that aging macaques develop tau pathology in a pattern and sequence qualitatively similar to human AD subjects.<sup>8</sup> Multilabel immunofluorescence labeling for pT217-tau and MAP2, and immunoperoxidase pT217-tau immunolabeling were used to determine the spatial and temporal progression of pT217-tau expression across the age span in rhesus macaque ERC layer II and dIPFC layer III. In adult (8–10 years) macaque, we observed pT217-tau expression within the nucleus in a subset of excitatory cells (Figure 1Ai-Ci, Di-Fi; Figure S1 in supporting information), which remained in aged animals (Figure 1Aii-Fiii; Supplement S1 Aii-Fiii; Figure S2 A-G in supporting information), including delicate expression in proximal apical dendrites and cell soma. Previous studies have identified an important role for tau in preventing genomic instability, rRNA transcription, and chromatin relaxation in the nucleus.<sup>41–43</sup> With advancing age, immunofluorescence revealed pT217-tau accumulating in proximal and more distal apical and basal dendrites in ERC layer II excitatory cells and dIPFC deep layer III pyramidal cells, both in “early” aged monkeys (18–19 years; Figure 1Aii-Cii, Dii-Fii; Figure S1) and “late” aged monkeys (28–34 years; Figure 1Aiii-Ciii, Diii-Fiii; Figure S1).

### 3.2 | Postsynaptic expression of pT217-tau in ERC and dIPFC in aging rhesus macaques

Ultrastructural analyses of “early” aged layer II ERC and “late” aged layer III dIPFC revealed that pT217-tau is concentrated in excitatory neurons in postsynaptic subcompartments within dendritic spines near asymmetric, glutamate-like synapses (Figure 2; Figure S3 in supporting information), and in dendritic shafts (Figure 3). In dendritic spines, pT217-tau is observed directly in association with the smooth endoplasmic reticulum (SER) spine apparatus near axospinous, presumed glutamatergic, asymmetric synapses, subjacent to the PSD and directly over the postsynaptic membrane (Figure 2). In dendrites, there was extensive pT217-tau aggregation along microtubules and on the SER; these dendrites had the characteristics of excitatory neuron dendritic shafts (Figure 3A-D). The accumulation of pT217-tau along



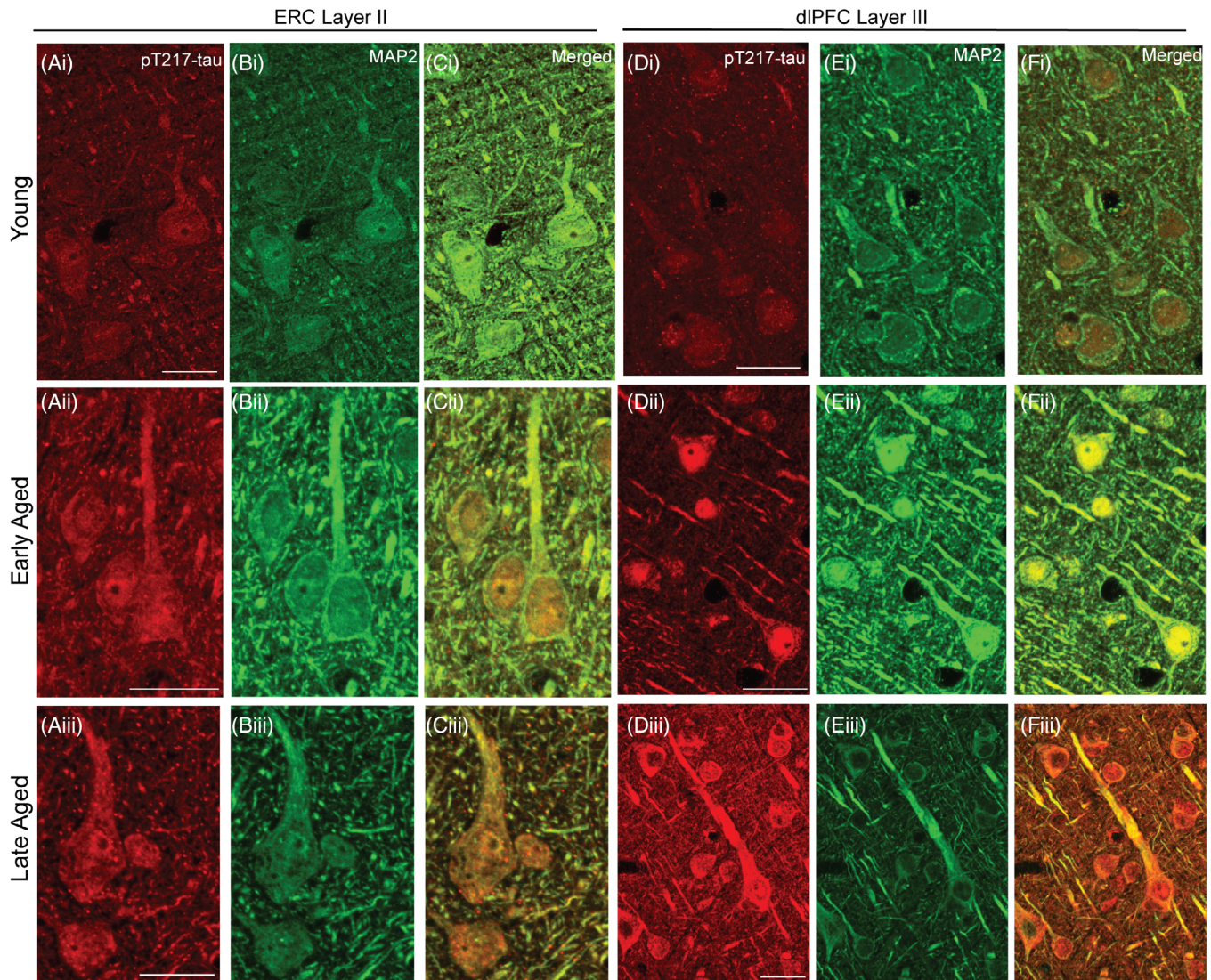


**FIGURE 1** Spatial and temporal localization pattern of pT217-tau across vulnerable cortical regions. Multiple-label immunofluorescence showing pT217-tau labeling (red) co-localized in excitatory neurons (MAP2, green) in ERC layer II and dIPFC layer III across age span in rhesus macaques at high magnification. In adult (8–10 years) rhesus macaques, pT217-tau immunolabeling was observed within the perisomatic compartment and the nucleus in a subset of excitatory cells (Ai–Ci, Di–Fi), including delicate expression in proximal apical dendrites in ERC layer II cell islands and dIPFC layer III microcircuits. With advancing age, immunofluorescence revealed pT217-tau accumulating in proximal and more distal apical and basal dendrites in ERC layer II excitatory cells and dIPFC deep layer III pyramidal cells, both in “early” aged monkeys (18–19 years; Aii–Cii, Dii–Fii) and “late” aged monkeys (28–34 years; Aiii–Ciii, Diii–Fiii). Scale bars: 24  $\mu$ m. dIPFC, dorsolateral prefrontal cortex; ERC, entorhinal cortex; pT217-tau, tau phosphorylated at threonine-217

microtubules is particularly relevant to the pathogenesis of AD, as hyperphosphorylation of tau induces detachment from microtubules and primes tau for hyperphosphorylation by GSK3 $\beta$ , leading ultimately to the formation of neurofibrillary tangles.<sup>44</sup>

### 3.3 | Quantitative analysis of pT217-tau in ERC layer II and dIPFC layer III neuropil

The ultrastructural location of pT217-tau in “early” aged layer II ERC and “late” aged layer III dIPFC neuropil of the rhesus macaque was determined using quantitative analyses with immunoperoxidase

labeling. Analysis of pT217-tau immunolabeled profiles revealed that pT217-tau was predominately expressed within dendritic shafts (ERC layer II: 43.73% [Figure 3E], dIPFC layer III: 43.46% [Figure 3F]), where it was aggregated on microtubules and on the calcium-storing SER, and associated with dendritic pathology: autophagic vacuolar degeneration, disrupted endosomal trafficking on microtubules, and abnormal mitochondria (see description below). Similarly, there was extensive labeling within dendritic spines receiving a Type I asymmetric glutamatergic-like synapse (ERC layer II: 35.93% [Figure 3E], dIPFC layer III: 39.39% [Figure 3F]). In contrast, there was significantly less immunolabeling in axons and glial subcompartments (<10% each; Figure 3E–F).



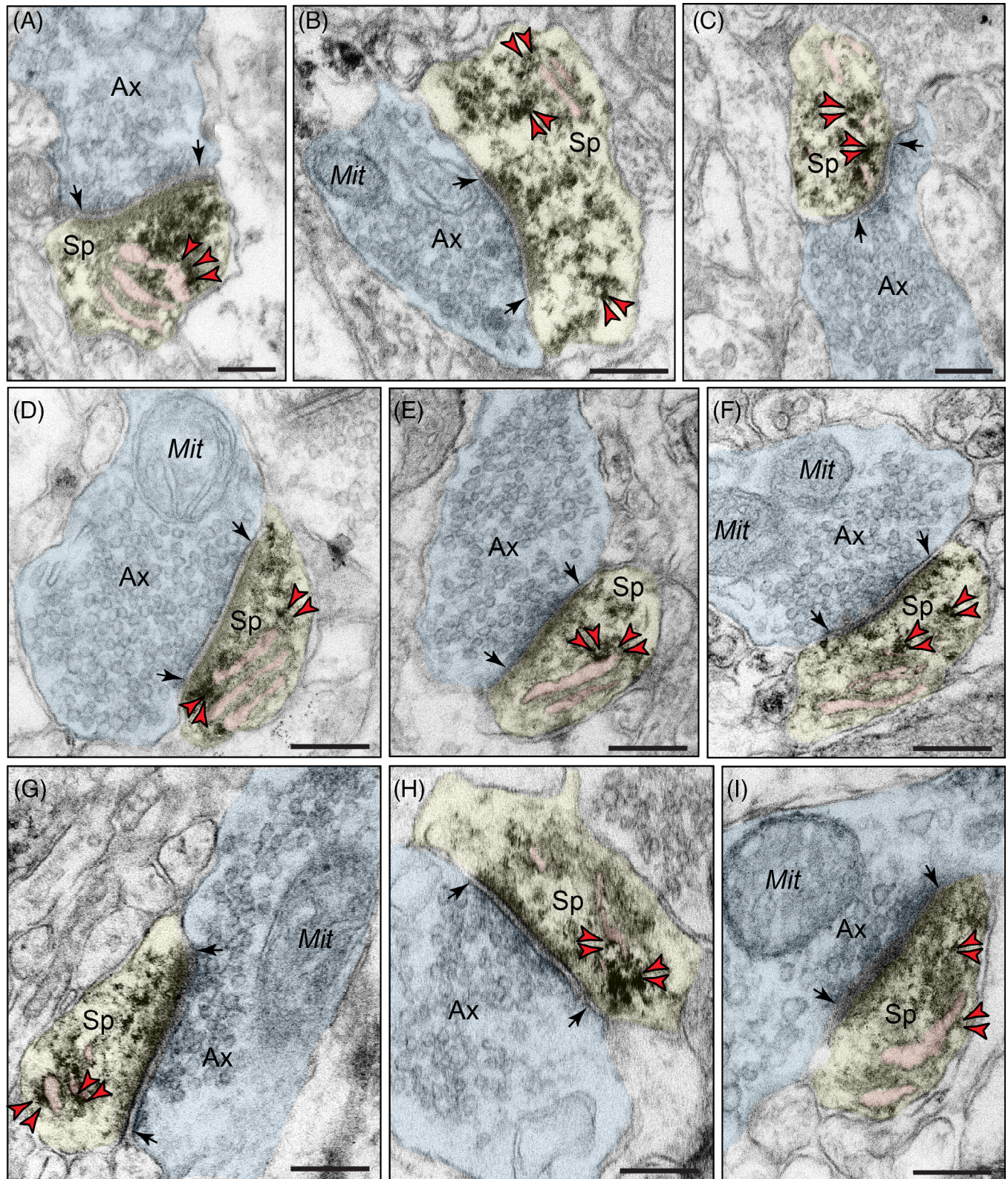


**FIGURE 2** Postsynaptic localization of pT217-tau in dendritic spines in rhesus macaque ERC and dlPFC. Immunoperoxidase labeling revealed that pT217-tau immunolabeling was concentrated in dendritic spines near asymmetric, glutamate-like synapses in rhesus macaque in “early” aged (18–24 years) macaque ERC layer II (A–C) and “late” aged (26–31 years) macaque dlPFC layer III (D–I). pT217-tau was observed directly in association with the smooth endoplasmic reticulum (SER) spine apparatus (pseudocolored pink). pT217-tau immunolabeling is also observed subjacent to the postsynaptic density, near axospinous, asymmetric glutamatergic synapses (A–C, D, F, G, I). Synapses are between arrows. Red arrowheads point to pT217-tau immunoreactivity. Profiles are pseudocolored for clarity. Scale bars, 200 nm. Ax, axon; dlPFC, dorsolateral prefrontal cortex; ERC, entorhinal cortex; Mit, mitochondria; pT217-tau, tau phosphorylated at threonine-217; Sp, dendritic spine



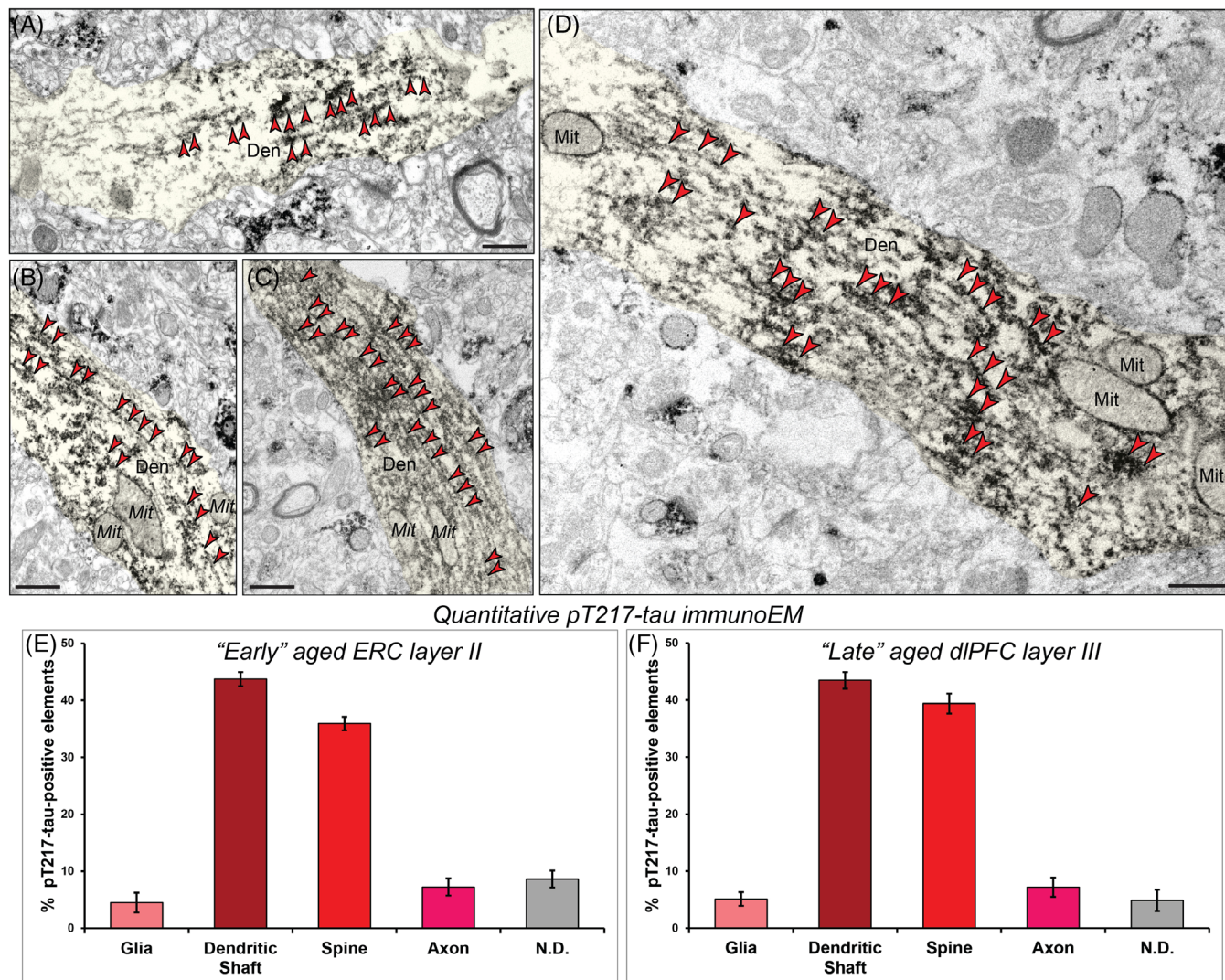


**FIGURE 3** Aggregation of pT217-tau along microtubules in dendritic shafts. ImmunoEM demonstrates aggregation of pT217-tau along dendritic microtubules in putative excitatory cells in “early” aged (18–24 years) macaque ERC layer II (A–B) and pyramidal cells in “late” aged (26–31 years) macaque dIPFC layer III (C–D). Ultrastructural examination revealed dense accumulation of pT217-tau occurring in parallel microtubule bundles in horizontal dendrites. Red arrowheads point to pT217-tau immunoreactivity. Profiles are pseudocolored for clarity. Scale bars, 200 nm. Quantitative analysis of pT217-tau immunoEM localization in rhesus macaque “early” aged (18–24 years) ERC layer II circuits (E). The prevalence of pT217-tau in various cellular subcompartments in layer II of the ERC neuropil, expressed as percentage of pT217-tau profile (e.g., dendrite) per total pT217-tau profiles. We analyzed a total of 1205 pT217-tau immunopositive profiles in “early” aged (18–24 years) ERC layer II neuropil. pT217-tau is primarily expressed in postsynaptic subcompartments in “early” aged (18–24 years) ERC layer II microcircuits, with foremost expression in dendritic shafts, and significant expression within dendritic spines. Quantitative analysis of pT217-tau immunoEM localization in rhesus macaque in “late” aged (26–31 years) macaque dIPFC layer III (F). The prevalence of pT217-tau in various cellular subcompartments in layer III of the dIPFC neuropil, expressed as percentage of pT217-tau profile (e.g., dendritic shaft) per total pT217-tau profiles. We analyzed a total of 1254 pT217-tau immunopositive profiles in “late” aged (26–31 years) macaque dIPFC layer III. pT217-tau is primarily expressed in postsynaptic subcompartments in dIPFC layer III microcircuits, with greatest expression in dendritic shafts, and significant expression within dendritic spines. For additional details regarding quantitative assessment and profile identification see Materials and Methods section. Nondetermined (N.D) are profiles that could not be unequivocally categorized. Den, dendrite; dIPFC, dorsolateral prefrontal cortex; ERC, entorhinal cortex; Mit, mitochondria; pT217-tau, tau phosphorylated at threonine-217

### 3.4 | pT217-tau “seeding” within vulnerable neuronal networks in AD

Various lines of evidence in human<sup>10,14–17</sup> and rodent studies<sup>17–25</sup> have provided evidence of phosphorylated tau trafficking to “seed” pathology in higher cortical networks subserving cognition. Immu-

noEM is the only method with sufficient, nanoscale resolution to allow actual visualization of this process *ex vivo*, and thus was of particular interest in the current study. As shown in Figure 4, aggregations of pT217-tau were observed within vesicular structures, including omega bodies fusing with the plasma membrane undergoing endo/exocytosis, within the postsynaptic membrane on dendritic spines in “early” aged



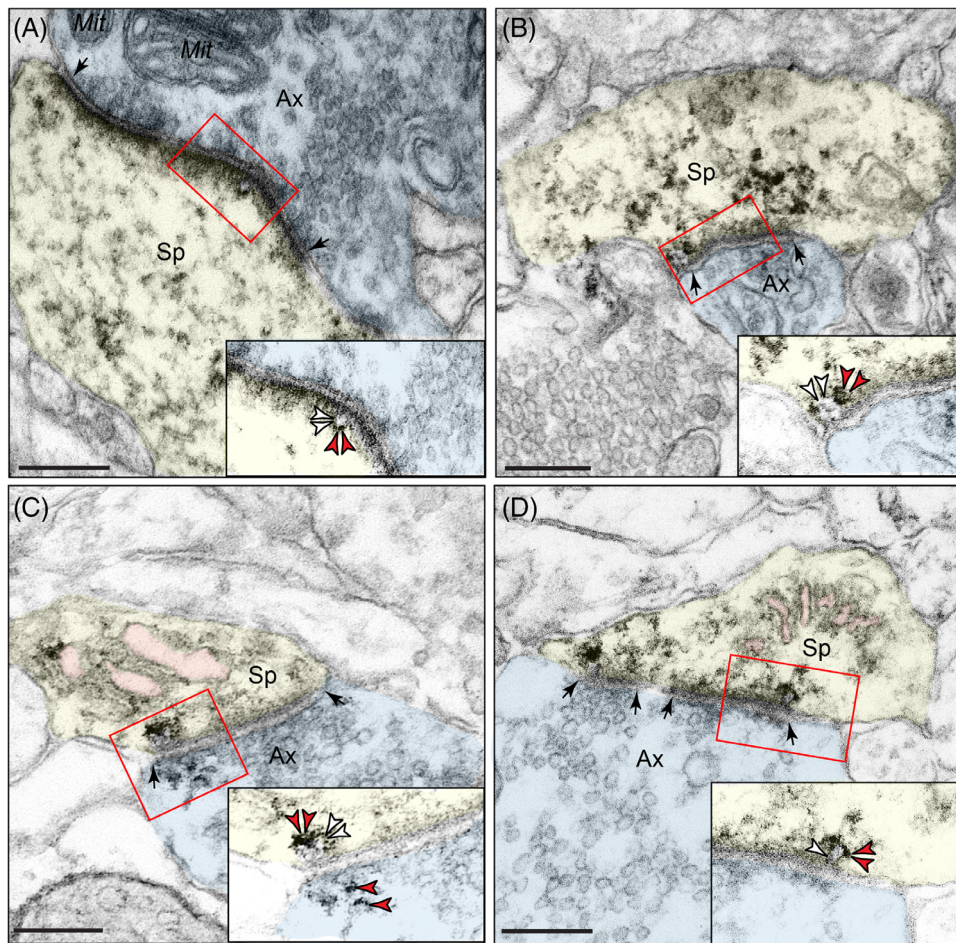


**FIGURE 4** Trans-synaptic trafficking of pT217-tau in aging rhesus macaques. Early-stage, soluble pT217-tau propagates between excitatory neurons within glutamate-like synapses in “early” aged (18–24 years) macaque ERC layer II (A–B) and in “late” aged (26–31 years) macaque dIPFC layer III (C–D). Trans-synaptic propagation of pT217-tau occurs via omega-shaped endosome-like vesicular profiles on the plasma membrane within dendritic spines, specifically within the synapse (insets). All dendritic spines receive axospinous Type I asymmetric glutamatergic-like synapses. Red arrowheads point to pT217-tau immunoreactivity. Black arrows point to the synapse; white arrowheads indicate an omega-shaped profile on the plasma membrane. The SER is pseudocolored in pink. Profiles are pseudocolored for clarity. Scale bars, 200 nm. Ax, axon; dIPFC, dorsolateral prefrontal cortex; ERC, entorhinal cortex; Mit, mitochondria; pT217-tau, tau phosphorylated at threonine-217; SER, smooth endoplasmic reticulum; Sp, dendritic spine

(18–24 years) macaque ERC layer II (Figure 4A–B) and in “late” aged (26–31 years) macaque dIPFC layer III (Figure 4C–D). In Figure 4C, pT217-tau could be seen next to both the postsynaptic and presynaptic membranes, consistent with pT217-tau trafficking between neurons to “seed” a network of tau pathology. It is noteworthy that pT217-tau was only visualized near excitatory (asymmetric), but not inhibitory (symmetric) synapses (Figure 4A–D), consistent with tau pathology afflicting glutamatergic, but not GABAergic, cortical neurons in AD.<sup>45</sup>

### 3.5 | Association of autophagic degeneration in pT217-tau immunopositive dendrites

A critical pathological hallmark in AD involves the formation of autophagic vacuoles, indicative of a degenerative cascade,<sup>46–48</sup> often-times in neurofibrillary tangle-containing neurons, leaving ultimately a “ghost tangle” in advanced stages of the illness. Our previous ultra-

structural studies have revealed that ERC layer II and dIPFC layer III neurons showed typical signs of AD-like degeneration, including large autophagic vacuoles in the soma and proximal apical and basilar dendrites.<sup>8,49</sup> We wanted to investigate whether these morphological aberrations are enriched in pT217-tau-immunopositive dendrites. ImmunoEM revealed that pT217-tau is co-localized with autophagic vacuoles in dendrites in “early” aged (18–24 years) macaque ERC layer II (Figure 5A–E) and in “late” aged (26–31 years) macaque dIPFC layer III (Figure 6A–E). Quantitative analyses determined that the vast majority of pT217-tau-expressing dendrites contained autophagic vacuoles. In ERC layer II, we analyzed a total of 116 profiles and found signatures of autophagic degeneration within a large proportion ( $N = 106$ ; 91%) of pT217-tau immunolabeled dendrites (Figure 5F). In dIPFC layer III, we analyzed a total of 82 profiles and found signatures of autophagic degeneration within a large proportion ( $N = 71$ ; 88%) of pT217-tau immunolabeled dendrites (Figure 6F). The robust association between pT217-tau immunopositivity and early signs of autophagic



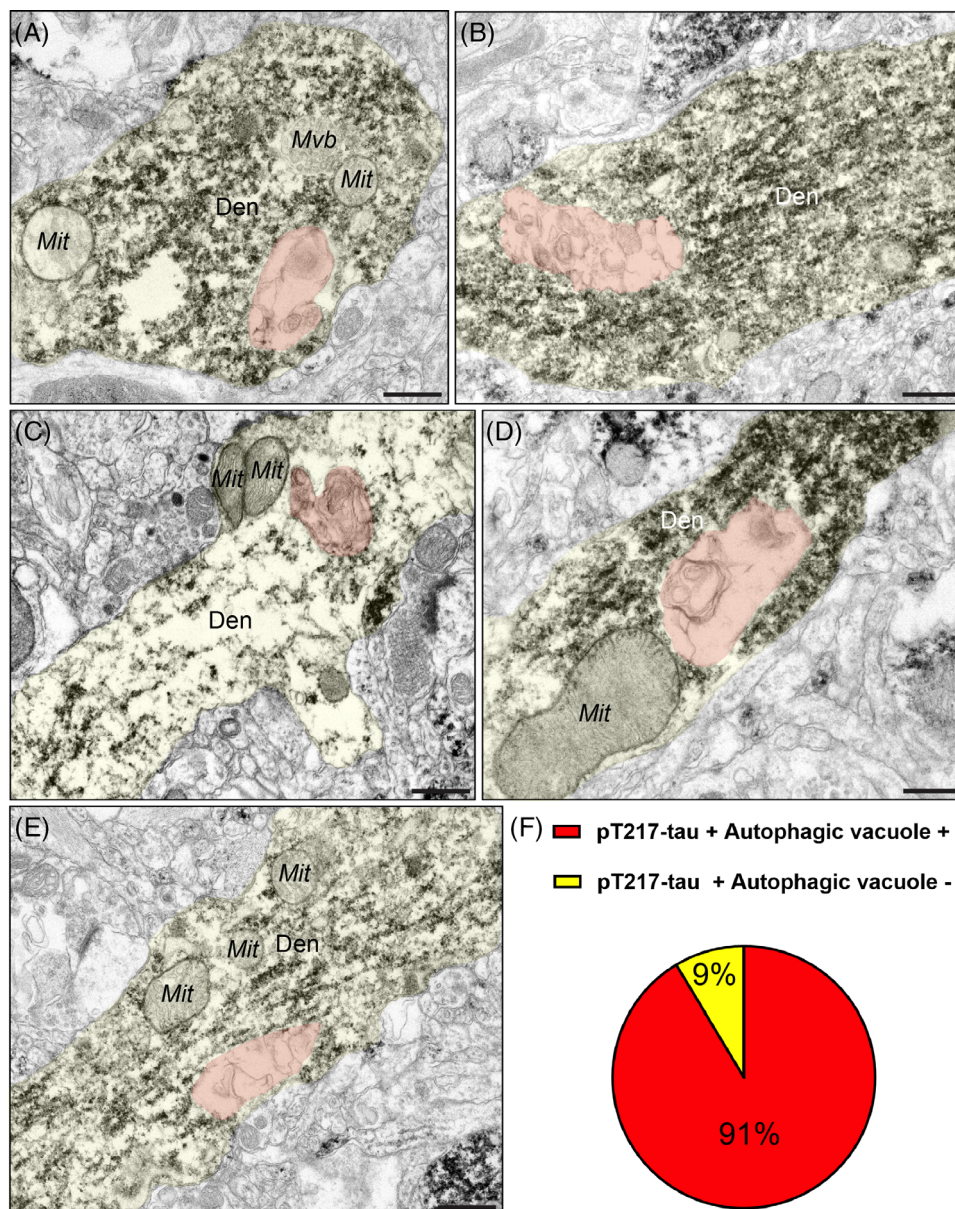


**FIGURE 5** Concomitant autophagic degeneration in pT217-tau immunopositive dendrites in ERC. Association of pT217-tau immunolabeling in degenerating dendrites containing autophagic vacuoles in ERC layer II (A-E). Autophagic vacuoles with multilamellar bodies (pseudocolored in orange) were observed in principal dendrites immunopositive for pT217-tau in “early” aged (18–24 years) rhesus macaque ERC layer II. Systematic quantification ( $N = 116$  profiles) in ERC layer II revealed robust concordance between signatures of autophagic degeneration and immunopositivity for pT217-tau ( $N = 106$ ; 91%) within dendrites (F). The percentage of pT217-tau-immunopositive dendrites showing signatures of autophagic degeneration is shown using a pie chart (F). Profiles are pseudocolored for clarity. Scale bars, 200 nm. Den, dendrite; dlPFC, dorsolateral prefrontal cortex; ERC, entorhinal cortex; Mit, mitochondria; pT217-tau, tau phosphorylated at threonine-217

degeneration within dendritic shafts may help to explain why plasma pT217-tau predicts future neurodegeneration and symptoms in humans.

### 3.6 | Aggregated pT217-tau on microtubules surrounds endosomes

Our previous data from aging rhesus monkeys purport a mechanism by which phosphorylated tau may exacerbate  $A\beta$  generation within neu-

rons, similar to how genetic predispositions in retromer (e.g., SORL1) signaling pathways may increase the risk of sporadic AD by triggering “endosomal traffic jams,” increasing the time amyloid precursor protein (APP) spends in endosomes where it is cleaved to  $A\beta$ .<sup>50</sup> Endosomes normally traffic on microtubules, providing anterograde and retrograde transport of cargo within cells. In aged macaques, endosomes labeled by EEA1 are often enlarged (Figure S4 in supporting information). The current data show that pT217-tau aggregations on dendritic microtubules surround endosomes in “early” aged (18–24 years) macaque ERC layer II and in “late” aged (26–31 years)



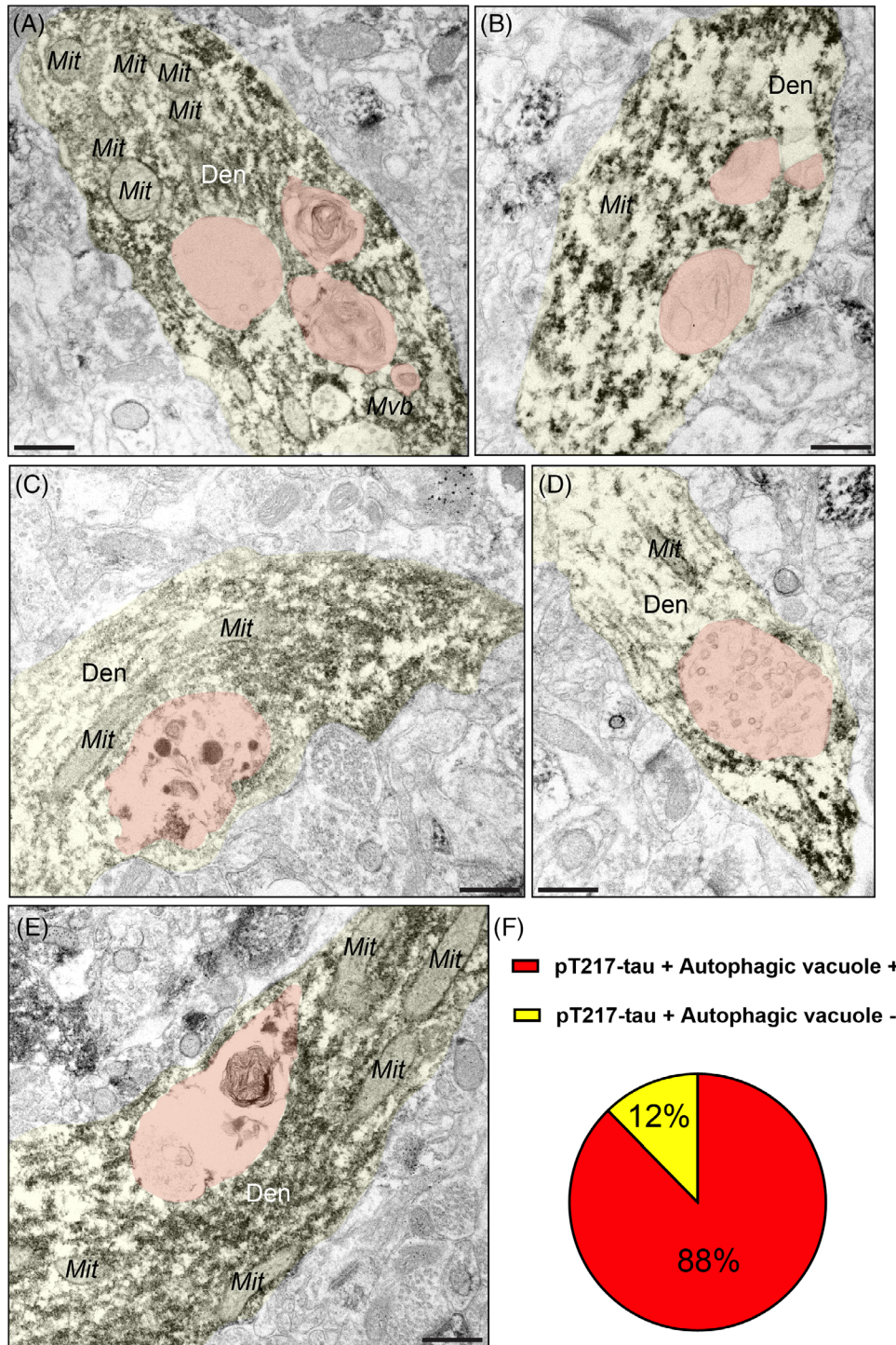


**FIGURE 6** Concomitant autophagic degeneration in pT217-tau immunopositive dendrites in dIPFC. Association of pT217-tau immunolabeling in degenerating dendrites containing autophagic vacuoles in dIPFC layer III (A-E). Autophagic vacuoles with multilamellar bodies (pseudocolored in orange) were observed in principal dendrites immunopositive for pT217-tau in pyramidal cells in “late” aged (26–31 years) macaque dIPFC layer III. Systematic quantification ( $N = 82$  profiles) in dIPFC layer III revealed robust concordance between signatures of autophagic degeneration and immunopositivity for pT217-tau ( $N = 71$ ; 88%) within dendrites (F). The percentage of pT217-tau-immunopositive dendrites showing signatures of autophagic degeneration is shown using a pie chart (F). Profiles are pseudocolored for clarity. Scale bars, 200 nm. Den, dendrite; dIPFC, dorsolateral prefrontal cortex; ERC, entorhinal cortex; Mit, mitochondria; pT217-tau, tau phosphorylated at threonine-217

macaque dIPFC layer III (Figure 7A-D). Using dual-label immunoEM, the current data show evidence of pT217-tau surrounding endosomes containing A $\beta$ 42 in dendrites in aged macaque dIPFC, suggesting that pT217-tau may be involved in the etiology of amyloid pathology (Figure 7C-D; Figure S5A-B in supporting information). We used the DAB immunoperoxidase approach to label pT217-tau, which provides sensitivity, and immunogold labeling to identify A $\beta$ 42, which permits precise spatial localization. We also observed evidence of pT217-tau and A $\beta$ 42 co-localized within dendrites with concordant signatures of autophagic vacuolar degeneration (Figure S5). This disruption of intracellular trafficking may contribute to dendritic pathology and may hasten the cleavage of A $\beta$  from APP (see Discussion). Consistent with dendritic pathology, pT217-tau immunolabeling was also associated with abnormal mitochondria, that is, mitochondria-on-a-string (MOAS) profiles (Figure 7A,E-G), that have previously been documented in both aging rhesus macaques and patients with AD.<sup>51-53</sup>

Previous studies of *post mortem* human AD brain showed that pT217-tau colocalized with Cki $\delta$ , a marker of granulovacuolar degeneration bodies (GVB).<sup>54</sup> Thus, we examined whether a similar relationship could be seen in aged macaque cortex. As with human AD tissue, we observed punctate vesicular-like patterns of Cki $\delta$ , co-localized with pT217-tau within apical dendrites and in the perisomatic compartment of pyramidal cells in "late" aged macaque dIPFC (Figure S6 in supporting information). Furthermore, previous studies have shown a strong relationship between pT217-tau and multivesicular bodies.<sup>54</sup> Our immunoEM data revealed a similar pattern in "early" aged (18-24 years) macaque ERC layer II and in "late" aged (26-31 years) macaque dIPFC layer III, showing an association between pT217-tau immunoperoxidase immunolabeling and morphologically identified multivesicular bodies (Figure S7 in supporting information).

### 3.7 | Age-related increases in pT217-tau in blood plasma in rhesus macaques

Plasma pT217-tau assays are showing promise as indices of brain pathology in humans.<sup>1</sup> The current study examined pT217-tau levels in the plasma of rhesus macaques across the entire macaque age span. As shown in Figure 8A, plasma levels of pT217-tau showed a significant positive correlation with age ( $R^2 = 0.2257$ ;  $P = 0.0099$ ) in rhesus macaques. Similarly, a groupwise comparison showed a statistically significant ( $P = 0.0405$ ) increase in pT217-tau in blood plasma in aged ( $\geq 18$  years) versus young ( $< 18$  years) animals (Figure 8B). These data suggest that plasma pT217-tau may also be used to track tau pathology in rhesus macaques, in which direct comparisons can be made to soluble pT217-tau brain levels, not possible in humans.

## 4 | DISCUSSION

Our immunoEM and multilabel immunofluorescence analyses of pT217-tau expression in aging rhesus macaque cortical tissue revealed robust expression in the cortical circuits vulnerable in AD. pT217-tau

was concentrated in the dendrites and dendritic spines of excitatory neurons in ERC layer II and dIPFC layer III, where it was aggregated on microtubules and on the calcium-storing SER (schematically illustrated in Figure 8C). As calcium dysregulation likely plays an important etiological role in driving tau hyperphosphorylation, the localization on the SER in dendritic spines and dendrites may be related to this mechanism. Particularly relevant to pT217-tau's role as an emerging fluid biomarker in AD, pT217-tau could be seen trafficking between neurons, where it was exposed to the extracellular space, and thus accessible to CSF and blood (Figure 8C). The association of pT217-tau with dendritic pathology: autophagic vacuolar degeneration, disrupted endosomal trafficking on microtubules, and abnormal mitochondria (Figure 8C), also helps to explain why plasma pT217-tau predicts future neurodegeneration and symptoms in humans. Finally, we found that plasma pT217-tau significantly increases across the age span in macaques, indicating that this animal model can help to illuminate the relationship between brain and plasma pT217-tau expression, and to test novel therapeutic interventions.

### 4.1 | Relevance to etiology of tau pathology in AD

Although *post mortem* human neuropathological studies have been critical in elucidating the spatial and temporal progression of tau pathology in AD, an important limitation is that these studies are predominantly able to capture fibrillated tau, as biochemical studies of fresh-frozen brain tissue have revealed that soluble phosphorylated tau is rapidly (within minutes) dephosphorylated *post mortem*.<sup>55</sup> In contrast, perfusion-fixation in rhesus macaques captures soluble early phosphorylated tau epitopes *in situ*, and thus allows visualization of the earliest stages of tau pathology that cannot be seen in human. Our data in rhesus macaques show that there is a prolonged stage of early tau pathology accumulation, thus providing an opportunity for timely intervention prior to neurodegeneration. Recent proteomic analyses of post-translational modifications (PTMs) of tau revealed that pT217-tau is a crucial, early phosphorylation epitope, distinguishing AD from other neurodegenerative disorders and indicative of disease progression.<sup>56</sup> Plasma and CSF measures of pT217-tau thus provide a rare window into emerging pathology in the human brain that cannot be seen with PET imaging or in *post mortem* human tissue, which predominantly capture late-stage, fibrillated forms of tau.<sup>57-60</sup> Our results reveal an age-related increase in plasma pT217-tau in rhesus macaques, suggesting that plasma pT217-tau can be used as an index of ensuing pathology in rhesus macaques as well, where future studies can directly examine how plasma levels relate to brain measures. They may also provide the opportunity to test novel therapeutic strategies without sacrificing invaluable aged macaques.

The current data are also consistent with emerging data showing that calcium dysregulation with increasing age and/or inflammation drives tau hyperphosphorylation in both animal models and in human patients.<sup>61</sup> pT217-tau was concentrated on the SER in dendritic spines and dendrites, which is the key source of intracellular calcium within neurons (Figure 8C). Abnormal calcium storage and release from the



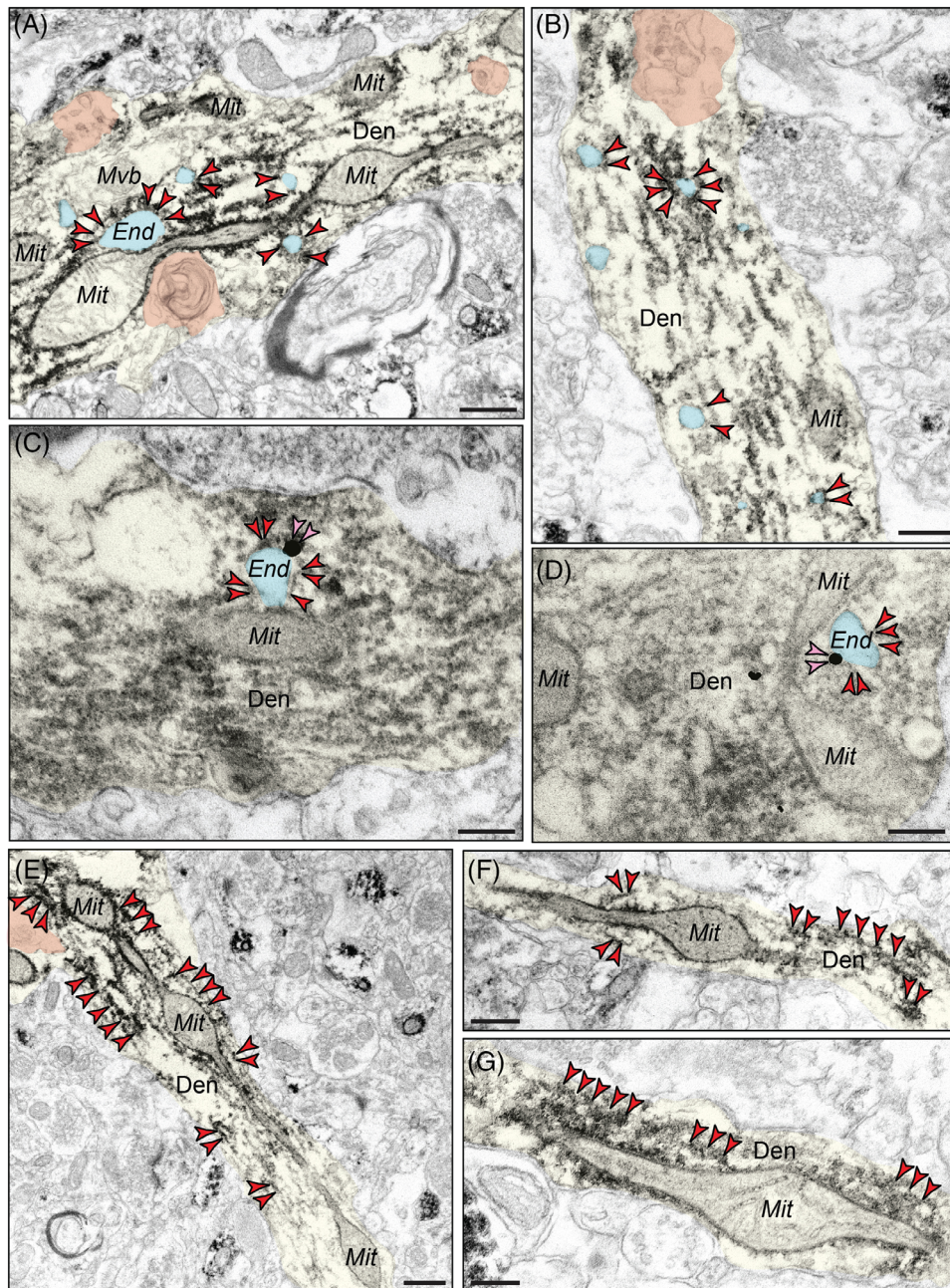


**FIGURE 7** Evidence of pT217-tau surrounding endosomes in dendritic shafts, oftentimes near dysmorphic mitochondrial profiles. pT217-tau (indicated by red arrowheads) aggregating on microtubules in dendrites where it surrounds enlarged endosomes (pseudocolored in cyan) in “early” aged (18–24 years) macaque ERC layer II and in “late” aged (26–31 years) macaque dIPFC layer III (A–D). Using dual-label immunoEM, the current data show evidence of pT217-tau surrounding endosomes containing A $\beta$ 42 (indicated by pink arrowheads) in dendrites in aged macaque dIPFC, suggesting that pT217-tau may be involved in the etiology of amyloid pathology (C–D). Aggregations of pT217-tau are often seen near dysmorphic mitochondria, characterized by MOAS morphological phenotypes, indicative of impaired mitochondrial fission and fusion (A, E–G). MOAS-like morphological disturbances have been described previously in aging rhesus macaques, consistent with local calcium dysregulation. Autophagic vacuolar degeneration (pseudocolored in orange) is also observed in several dendritic shafts, consistent with signatures of neurite dystrophy (A, B, E). Profiles are pseudocolored for clarity. Scale bars, 200 nm. A $\beta$ , amyloid beta; Den, dendrite; dIPFC, dorsolateral prefrontal cortex; End, endosome; ERC, entorhinal cortex; Mit, mitochondria; MOAS, mitochondria on a string; pT217-tau, tau phosphorylated at threonine-217

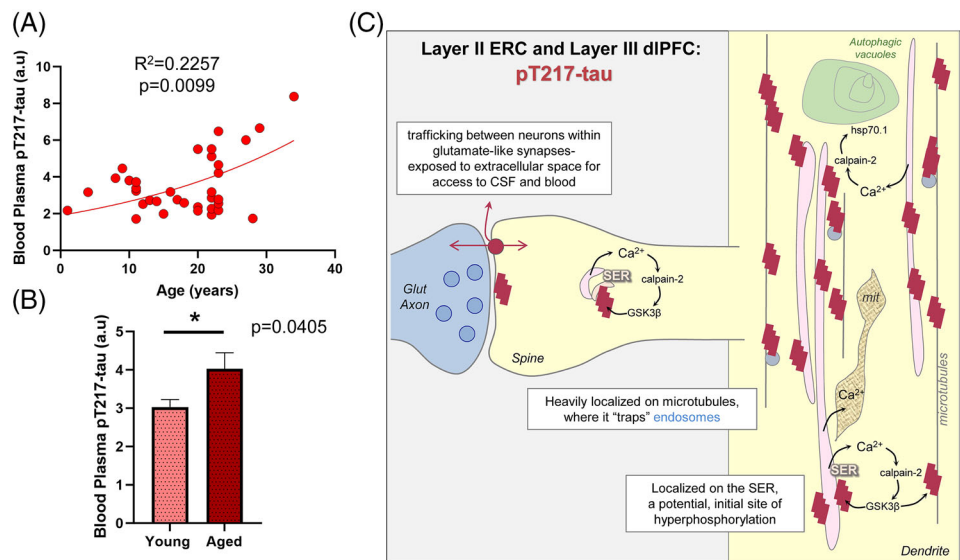


**FIGURE 8** Increased pT217-tau in blood plasma in aging rhesus macaques, and a working model of pT217-tau etiology and toxic actions. Age-related elevation in pT217-tau in blood plasma in aging rhesus macaques (A). Results from a regression analysis performed in all animals ( $N = 36$ ) indicated statistically significant increases in pT217-tau signal with advancing age ( $R^2 = 0.2257$ ,  $P = 0.0099$ ). Quantification of pT217-tau in blood plasma grouped by age (B). Young animals ( $N = 15$ ) are compared to aged animals ( $N = 21$ ) via a two-tailed Welch t test ( $*P = 0.0405$ ). SEM is plotted for each group. Summary schematic of pT217-tau expression patterns in "early" aged (18–24 years) macaque ERC layer II and in "late" aged (26–31 years) macaque dlPFC layer III microcircuits (C). A schematic illustration of pT217-tau localization in dendrites, and its potential etiology and toxic actions. pT217-tau is primarily located in glutamatergic dendrites and dendritic spines, consistent with the known origins of tau pathology in dendrites in humans.<sup>45</sup> The current study found evidence of pT217-tau trafficking between neurons at glutamate-like synapses, interfacing with the extracellular space to become accessible in CSF and plasma. This may contribute to tau "seeding" pathology through an interconnected network of glutamatergic neurons. Aggregations of pT217-tau were prominently expressed on microtubules, as well as on the calcium-storing SER, where increased calcium release may drive GSK3 $\beta$  hyperphosphorylation of tau at T217. These dendrites often showed signs of pathology: autophagic vacuoles that are an early sign of autophagic degeneration and abnormal mitochondria (mit), known as MOAS. The aggregations of pT217-tau on microtubules could be seen to "trap" endosomes, interfering with intracellular trafficking needed for healthy dendrites. These "endosomal traffic jams" may also increase the production of A $\beta$  by increasing the time APP spends in endosomes with exposure to  $\beta$ -secretase, a hypothesis to be tested in future research. A $\beta$ , amyloid beta; APP, amyloid precursor protein; CSF, cerebrospinal fluid; dlPFC, dorsolateral prefrontal cortex; End, endosome; ERC, entorhinal cortex; Mit, mitochondria; MOAS, mitochondria on a string; pT217-tau, tau phosphorylated at threonine-217; SEM, standard error of the mean; SER, smooth endoplasmic reticulum

SER is evident in both sporadic and inherited AD,<sup>62</sup> in which high levels of cytosolic calcium drive calpain-2-mediated disinhibition of GSK3 $\beta$  and cdk5 to hyperphosphorylate tau,<sup>21,63–65</sup> including at pT217-tau.<sup>66</sup> As tau is normally localized on microtubules, these toxic actions in dendrites would hyperphosphorylate tau on microtubules, causing tau to detach and aggregate, as seen in the current study. The data also show that aggregations of pT217-tau along microtubules "trap" endosomes, interfering with intracellular trafficking needed for healthy dendrites, and which may contribute to amyloid pathology<sup>7</sup> as discussed below.

#### 4.2 | Visualization of tau seeding and relationship to pT217-tau as a plasma biomarker

The current data help to demonstrate how pT217-tau transfers from within neurons to the extracellular space where it can be conveyed to CSF and plasma for detection as a fluid biomarker. ImmunoEM is the only method with sufficiently high resolution to visualize the pT217-tau trafficking between neurons in its native state. This is likely a momentary event, and thus capturing the event in process is fortuitous

and rare. The data reveal that pT217-tau gets exposed to the extracellular space during this process, and thus may be conveyed to CSF and plasma. It is important to note that this is an early event, suggesting that the seeding of tau pathology between neurons likely occurs at an early stage when phosphorylated tau is still soluble. It is also noteworthy that this study, as well as our previous work with pS214-tau,<sup>67</sup> have only seen this occur in or near glutamatergic (asymmetric) synapses, but not GABAergic (symmetric) synapses, consistent with tau spreading from the ERC to "infect" interconnected cortical networks.<sup>45</sup>

The current data suggest that phosphorylated tau may need to be in a flexible state, for example, in soluble form, to effectively transfer between neurons. In contrast, fibrillated tau labeled with the AT8 antibody has a markedly different appearance, with long, inflexible fibrils (>200 nm)<sup>8</sup> that would not be amenable to trafficking within the smaller ( $\approx 100$  nm) vesicle-like structures observed here. Consistent with our findings, recent studies have revealed evidence of pT217-tau vesicular structures associated within GVB large membrane-bound vacuoles containing aggregated proteins including phosphorylated tau.<sup>54</sup> GVBs are correlated with the spatial and temporal propagation of tau pathology.<sup>68</sup> Future studies can delineate



whether trans-synaptic trafficking of pT217-tau depends upon low-density lipoprotein receptor-related protein 1 (LRP1)<sup>69</sup> and bridging integrator 1 (BIN1),<sup>70</sup> which have been shown to be important for the interneuronal trafficking of tau. Altogether, these data from non-human primate brains indicate how tau pathology can spread over a lifetime, starting early and eventually compromising the integrity of higher cortical networks.<sup>7</sup>

### 4.3 | Relevance for the prediction of clinical progression and pathology in AD

Recent research has shown that plasma pT217-tau discriminates AD from other neurodegenerative diseases, with high accuracy similar to key CSF- or PET-based measures.<sup>1</sup> In autosomal dominant AD, pT217-tau begins with the initial increases in aggregated A $\beta$  as early as two decades before the development of aggregated tau pathology<sup>2</sup> and symptom onset.<sup>1,2</sup> In sporadic AD, pT217-tau is already associated with fibrillar amyloid deposition in the earliest presymptomatic stages beginning at subthreshold amyloid levels (20 Centiloids).<sup>71</sup> Moreover, in emerging longitudinal studies, plasma pT217-tau has been associated with cognitive decline in patients with preclinical AD.<sup>3</sup> Finally, plasma pT217-tau—among multiple tau species and other biomarkers—has demonstrated the highest accuracy to predict the presence of AD neuropathology, including aggregated tau pathology.<sup>4</sup>

The current data help to illuminate why this tau species is so predictive, as it is expressed in dendrites that show signs of early degeneration, including autophagic vacuoles and abnormal mitochondria. These degenerative signs may also be related to calcium dysregulation, for example, where calpain cleaves heat shock protein Hsp70.1 to increase autophagic neurodegeneration<sup>72</sup> (Figure 8C). In AD, autophagic vacuoles are found in AT8-labeled neurons indicative of a degenerative cascade,<sup>46–48</sup> eventually leaving a residual “ghost” tangle.<sup>73</sup> Thus, pT217-tau in plasma may serve as an early index of dendrites initiating the degenerative process.<sup>74</sup> Our preliminary observations with multiple-label immunofluorescence shows pT217-tau labeling co-localized in pyramidal neurons with AT8 in “late” aged (26–31 years) macaque dlPFC layer III (Figure S8 in supporting information). Future studies will elucidate the spatial and temporal sequence of multiple phosphorylated tau epitopes in vulnerable cortical circuits in AD, and whether these occur concurrently in the same cell types, especially comparing early-stage, soluble phosphorylated tau epitopes to late-stage, fibrillated markers (e.g., thioflavin S, paired helical filament-1 [PHF-1]).

### 4.4 | pT217-tau “trapping” endosomes in dendritic shafts: Potential interaction between tau phosphorylation and A $\beta$

Extensive research has shown that A $\beta$  cleavage from APP is increased when APP is expressed in endosomes, as they often contain beta secretase, the crucial factor for A $\beta$  production.<sup>75</sup> Indeed, the increased

risk of AD from genetic alterations in retromer-dependent signaling (e.g., SORL1, VPS26, VPS35) is thought to involve this mechanism, by which “endosomal traffic jams” increase APP time spent in endosomes where it is cleaved to A $\beta$ .<sup>50</sup> Our data have suggested that aggregations of phosphorylated tau on microtubules may have a similar effect, “trapping” endosomes to create a similar “traffic jam”<sup>7</sup> including immunoEM evidence of AT8-labeled phosphorylated tau “trapping” endosomes labeled with APP.<sup>8</sup> The current data show extensive pT217-tau “trapping” endosomes, including endosomes associated with A $\beta$ 42, suggesting that pT217-tau may be involved in the etiology of amyloid pathology. This hypothesis may help to explain why plasma pT217-tau levels correlate so highly with amyloid pathology in humans.<sup>60,76</sup> Although it is widely considered that A $\beta$  drives tau phosphorylation, the current data suggest that the converse may also be true and that the extensive aggregation of pT217-tau on microtubules may help to explain the correlation with this particular phosphorylated tau species. Consistent with this hypothesis, studies of anti-tau targeting antibodies are finding potential reductions in A $\beta$  as well as tau.<sup>77,78</sup>

In closing, these studies in aged monkeys help to reveal the cell biological processes associated with pT217-tau in ways not possible in human tissue. The data are consistent with pT217-tau having access to the extracellular space to serve as a fluid biomarker that predicts emerging degenerative pathology in the circuits most vulnerable in AD.

### AUTHOR CONTRIBUTIONS

DD designed and performed the experiments in immunohistochemistry and immunoEM. DD, MKPJ, and DW collected and analyzed immunoEM and immunohistochemistry experiments. IP and DD collected and analyzed multi-label immunofluorescence experiments. FL and ZX conducted plasma experiments. YMM, JA, and AD contributed to the experimental design and provided technical expertise. CHvD provided invaluable material resources and revised the manuscript. AFTA and DD designed the experiments, supervised the study, and wrote the manuscript. All authors read and approved the final manuscript.

### ACKNOWLEDGMENTS

We thank Lisa Ciavarella, Sam Johnson, Tracy Sadlon, and Michelle Wilson for their invaluable technical assistance. We are grateful to Heiko Braak and Kelly del Tredici for their constructive critiques and thoughtful suggestions. The authors also would like to thank the Center for Cellular and Molecular Imaging Microscopy Facility at Yale Medical School for assistance with the work presented here. This work was primarily supported by National Institutes of Health (NIH) R21 grant AG079145-01 to DD and RO1 grant AG061190-01 to AFTA. The work was also partially supported by the American Federation for Aging Research (AFAR) Faculty Transition Award and support from Yale Alzheimer's Disease Research Center (ADRC) P30AG066508 Pilot Project and Research Scholar Award to DD, support from the Alzheimer's Disease Research Unit (CHvD), and the MacBrain Resource Center (NIH MH113257 to AD). The measurement of pT217-tau was partially supported by Anesthesia Biomarker Core

at Massachusetts General Hospital and by NIH R01 AG RF1AG070761 grant to ZX.

### CONFLICT OF INTEREST STATEMENT

Dr. Zhongcong Xie provided consulting service to Baxter pharmaceutical company; Shanghai 9th and 10th hospitals; NanoMosaic, Inc.; and Anesthesiology and Perioperative Science in the past 36 months. All other co-authors have nothing to disclose. Author disclosures are available in the [supporting information](#).

### CONSENT STATEMENT

Consent was not necessary as no human subjects were involved in any studies.

### ORCID

Dibyadeep Datta  <https://orcid.org/0000-0002-5415-3067>

### REFERENCES

- Palmqvist S, Janelidze S, Quiroz YT, et al. Discriminative accuracy of plasma phospho-tau217 for Alzheimer disease vs other neurodegenerative disorders. *JAMA*. 2020;324:772-781.
- Barthelemy NR, Li Y, Joseph-Mathurin N, et al. A soluble phosphorylated tau signature links tau, amyloid and the evolution of stages of dominantly inherited Alzheimer's disease. *Nat Med*. 2020;26:398-407.
- Mattsson-Carlgen N, Salvado G, et al. Prediction of longitudinal cognitive decline in preclinical Alzheimer disease using plasma biomarkers. *JAMA Neurol*. 2023;30:360-369.
- Salvado G, Ossenkoppele R, Ashton NJ, et al. Specific associations between plasma biomarkers and postmortem amyloid plaque and tau tangle loads. *EMBO Mol Med*. 2023;15:e17123.
- Hansson O, Blennow K, Zetterberg H, Dage J. Blood biomarkers for Alzheimer's disease in clinical practice and trials. *Nat Aging*. 2023;3:506-519.
- Olsson B, Lautner R, Andreasson U, et al. CSF and blood biomarkers for the diagnosis of Alzheimer's disease: a systematic review and meta-analysis. *Lancet Neurol*. 2016;15:673-684.
- Arnsten AFT, Datta D, Del Tredici K, Braak H. Hypothesis: tau pathology is an initiating factor in sporadic Alzheimer's disease. *Alzheimers Dement*. 2021;17:115-124.
- Paspalas CD, Carlyle BC, Leslie S, et al. The aged rhesus macaque manifests Braak stage III/IV Alzheimer's-like pathology. *Alzheimers Dement*. 2018;14:680-691.
- Braak H, Del Tredici K. The preclinical phase of the pathological process underlying sporadic Alzheimer's disease. *Brain*. 2015;138:2814-2833.
- Braak H, Del Tredici K. Spreading of tau pathology in sporadic Alzheimer's disease along cortico-cortical top-down connections. *Cereb Cortex*. 2018;28:3372-3384.
- Braak H, Del Tredici K. Neuroanatomy and pathology of sporadic Alzheimer's disease. *Adv Anat Embryol Cell Biol*. 2015;215:1-162.
- La Joie R, Ayakta N, Seeley WW, Borys E, Boxer A, et al. Multisite study of the relationships between antemortem [11C]PIB-PET Centiloid values and postmortem measures of Alzheimer's disease neuropathology. *Alzheimers Dement*. 2019;15:205-216.
- Giannakopoulos P, Herrmann FR, Bussièrè T, et al. Tangle and neuron numbers, but not amyloid load, predict cognitive status in Alzheimer's disease. *Neurology*. 2003;60:1495-1500.
- Braak H, Zetterberg H, Del Tredici K, Blennow K. Intraneuronal tau aggregation precedes diffuse plaque deposition, but amyloid-beta changes occur before increases of tau in cerebrospinal fluid. *Acta Neuropathol*. 2013;126:631-641.
- Kaufman SK, Del Tredici K, Thomas TL, Braak H, Diamond MI. Tau seeding activity begins in the transentorhinal/entorhinal regions and anticipates phospho-tau pathology in Alzheimer's disease and PART. *Acta Neuropathol*. 2018;136:57-67.
- Vogel JW, Iturria-Medina Y, Strandberg OT, et al. Spread of pathological tau proteins through communicating neurons in human Alzheimer's disease. *Nat Commun*. 2020;11:2612.
- Vogels T, Leuzy A, Cicognola C, et al. Propagation of tau pathology: integrating insights from postmortem and in vivo studies. *Biol Psychiatry*. 2020;87:808-818.
- Ahmed Z, Cooper J, Murray TK, et al. A novel in vivo model of tau propagation with rapid and progressive neurofibrillary tangle pathology: the pattern of spread is determined by connectivity, not proximity. *Acta Neuropathol*. 2014;127:667-683.
- Calafate S, Buist A, Miskiewicz K, et al. Synaptic contacts enhance cell-to-cell tau pathology propagation. *Cell Rep*. 2015;11:1176-1183.
- Fu H, Hardy J, Duff KE. Selective vulnerability in neurodegenerative diseases. *Nat Neurosci*. 2018;21:1350-1358.
- Vasconcelos B, Stancu IC, Buist A, et al. Heterotypic seeding of Tau fibrillization by pre-aggregated Abeta provides potent seeds for prion-like seeding and propagation of Tau-pathology in vivo. *Acta Neuropathol*. 2016;131:549-569.
- Wu JW, Hussaini SA, Bastille IM, et al. Neuronal activity enhances tau propagation and tau pathology in vivo. *Nat Neurosci*. 2016;19:1085-1092.
- DeVos SL, Miller RL, Schoch KM, et al. Tau reduction prevents neuronal loss and reverses pathological tau deposition and seeding in mice with tauopathy. *Sci Transl Med*. 2017;9:eaag0481. doi:10.1126/scitranslmed.aag0481
- Holmes BB, Furman JL, Mahan TE, et al. Proteopathic tau seeding predicts tauopathy in vivo. *Proc Natl Acad Sci USA*. 2014;111:E4376-E4385.
- de Calignon A, Polydoro M, Suarez-Calvet M, et al. Propagation of tau pathology in a model of early Alzheimer's disease. *Neuron*. 2012;73:685-697.
- Paspalas CD, Wang M, Arnsten AFT. Constellation of HCN Channels and cAMP regulating proteins in dendritic spines of the primate prefrontal cortex — Potential substrate for working memory deficits in schizophrenia. *Cereb Cortex*. 2013;23:1643-1654.
- Jin LE, Wang M, Galvin VC, et al. mGluR2 vs. mGluR3 in Primate Prefrontal Cortex: postsynaptic mGluR3 Strengthen Cognitive Networks. *Cereb Cortex*. 2018;28:974-987.
- Datta D, Enwright JF, Arion D, et al. Mapping phosphodiesterase 4D (PDE4D) in macaque dorsolateral prefrontal cortex: postsynaptic compartmentalization in higher-order layer III pyramidal cell circuits. *Front Neuroanat*. 2020;14:578483.
- Datta D, Leslie SN, Wang M, et al. Age-related calcium dysregulation linked with tau pathology and impaired cognition in non-human primates. *Alzheimers Dement*. 2021;17:920-932.
- Ercan-Herbst E, Ehrig J, Schondorf DC, et al. A post-translational modification signature defines changes in soluble tau correlating with oligomerization in early stage Alzheimer's disease brain. *Acta Neuropathol Commun*. 2019;7:192.
- Gu J, Xu W, Jin N, et al. Truncation of Tau selectively facilitates its pathological activities. *J Biol Chem*. 2020;295:13812-13828.
- Javonillo DI, Tran KM, Phan J, et al. Systematic phenotyping and characterization of the 3xTg-AD mouse model of Alzheimer's disease. *Front Neurosci*. 2021;15:785276.
- Karikari TK, Emersic A, Vrillon A, et al. Head-to-head comparison of clinical performance of CSF phospho-tau T181 and T217 biomarkers for Alzheimer's disease diagnosis. *Alzheimers Dement*. 2021;17:755-767.
- Zhou Y, Shi J, Chu D, et al. Relevance of phosphorylation and truncation of tau to the etiopathogenesis of Alzheimer's disease. *Front Aging Neurosci*. 2018;10:27.

35. Moloney CM, Labuzan SA, et al. Phosphorylated tau sites that are elevated in Alzheimer's disease fluid biomarkers are visualized in early neurofibrillary tangle maturity levels in the post mortem brain. *Alzheimers Dement*. 2022
36. Peters A, Palay SL, Webster HD. *The fine structure of the nervous system: neurons and their supporting cells*. Oxford Univ. Press; 1991
37. Yang S, Datta D, Elizabeth W, et al. Inhibition of glutamate-carboxypeptidase-II in dorsolateral prefrontal cortex: potential therapeutic target for neuroinflammatory cognitive disorders. *Mol Psychiatry*. 2022;27:4252-4263.
38. Liang F, Clarke N, Patel P, Loncar M, Quan Q. Scalable photonic crystal chips for high sensitivity protein detection. *Opt Express*. 2013;21:32306-32312.
39. Liang F, Baldyga K, Quan Q, Khatri A, Choi S, Wiener-Kronish J, et al. Preoperative plasma tau-PT217 and Tau-PT181 are associated with postoperative delirium. *Ann Surg*. 2022. <https://pubmed.ncbi.nlm.nih.gov/35794069/>
40. Lu J, Liang F, Bai P, et al. Blood tau-PT217 contributes to the anesthesia/surgery-induced delirium-like behavior in aged mice. *Alzheimers Dement*. 2023;19:4110-4126.
41. Bukar Maina M, Al-Hilaly YK, Serpell LC. Nuclear tau and its potential role in Alzheimer's disease. *Biomolecules*. 2016;6:9.
42. Ulrich G, Salvade A, Boersema P, et al. Phosphorylation of nuclear Tau is modulated by distinct cellular pathways. *Sci Rep*. 2018;8:17702.
43. Diez L, Wegmann S. Nuclear transport deficits in tau-related neurodegenerative diseases. *Front Neurol*. 2020;11:1056.
44. Liu SJ, Zhang JY, Li HL, et al. Tau becomes a more favorable substrate for GSK-3 when it is prephosphorylated by PKA in rat brain. *J Biol Chem*. 2004;279:50078-50088.
45. Braak H, Del Tredici K. Neuroanatomy and pathology of sporadic Alzheimer's disease. *Adv Anat Embryol Cell Biol*. 2015;215:1-162.
46. Nixon RA. Autophagy, amyloidogenesis and Alzheimer disease. *J Cell Sci*. 2007;120:4081-4091.
47. Orr ME, Oddo S. Autophagic/lysosomal dysfunction in Alzheimer's disease. *Alzheimers Res Ther*. 2013;5:53.
48. Piras A, Collin L, Gruninger F, Graff C, Ronnback A. Autophagic and lysosomal defects in human tauopathies: analysis of post-mortem brain from patients with familial Alzheimer disease, corticobasal degeneration and progressive supranuclear palsy. *Acta Neuropathol Commun*. 2016;4:22.
49. Arnsten AFT, Datta D, Tredici KD, Braak H. Hypothesis: tau pathology is an initiating factor in sporadic Alzheimer's disease. *Alzheimers Dement*. 2020
50. Small SA, Simoes-Spassov S, Mayeux R, Petsko GA. Endosomal traffic jams represent a pathogenic hub and therapeutic target in Alzheimer's disease. *Trends Neurosci*. 2017;40:592-602.
51. Datta D. Interrogating the etiology of sporadic Alzheimer's disease using aging rhesus macaques: cellular, molecular and cortical circuitry perspectives. *J Gerontol A Biol Sci Med Sci*. 2023;78(9):1523-1534.
52. Morozov YM, Datta D, Paspalas CD, Arnsten AFT. Ultrastructural evidence for impaired mitochondrial fission in the aged rhesus monkey dorsolateral prefrontal cortex. *Neurobiol Aging*. 2017;51:9-18.
53. Zhang L, Trushin S, Christensen TA, et al. Altered brain energetics induces mitochondrial fission arrest in Alzheimer's. *Disease Sci Rep*. 2016;6:18725.
54. Wennstrom M, Janelidze S, Nilsson KPR, et al. Cellular localization of p-tau217 in brain and its association with p-tau217 plasma levels. *Acta Neuropathol Commun*. 2022;10:3.
55. Wang Y, Zhang Y, Hu W, et al. Rapid alteration of protein phosphorylation during postmortem: implication in the study of protein phosphorylation. *Sci Rep*. 2015;5:15709.
56. Wesseling H, Mair W, Kumar M, et al. Tau PTM profiles identify patient heterogeneity and stages of Alzheimer's disease. *Cell*. 2020;183:1699-1713.
57. Janelidze S, Stomrud E, Smith R, et al. Cerebrospinal fluid p-tau217 performs better than p-tau181 as a biomarker of Alzheimer's disease. *Nat Commun*. 2020;11:1683.
58. Barthelemy NR, Bateman RJ, Hirtz C, et al. Cerebrospinal fluid phospho-tau T217 outperforms T181 as a biomarker for the differential diagnosis of Alzheimer's disease and PET amyloid-positive patient identification. *Alzheimers Res Ther*. 2020;12:26.
59. Mattsson-Carlsson N, Andersson E, et al. Abeta deposition is associated with increases in soluble and phosphorylated tau that precede a positive Tau PET in Alzheimer's disease. *Sci Adv*. 2020;6:eaaz2387.
60. Janelidze S, Berron D, Smith R, et al. Associations of plasma phospho-tau217 levels with tau positron emission tomography in early Alzheimer disease. *JAMA Neurol*. 2021;78:149-156.
61. Alzheimer's Association CHW. Calcium Hypothesis of Alzheimer's disease and brain aging: a framework for integrating new evidence into a comprehensive theory of pathogenesis. *Alzheimers Dement*. 2017;13:178-182.e17.
62. LaFerla FM. Calcium dyshomeostasis and intracellular signalling in Alzheimer's disease. *Nat Rev Neurosci*. 2002;3:862-872.
63. Grynspan F, Griffin WR, Cataldo A, Katayama S, Nixon RA. Active site-directed antibodies identify calpain II as an early-appearing and pervasive component of neurofibrillary pathology in Alzheimer's disease. *Brain Res*. 1997;763:145-158.
64. Saito K, Elce JS, Hamos JE, Nixon RA. Widespread activation of calcium-activated neutral proteinase (calpain) in the brain in Alzheimer disease: a potential molecular basis for neuronal degeneration. *Proc Natl Acad Sci USA*. 1993;90:2628-2632.
65. Kurbatskaya K, Phillips EC, Croft CL, et al. Upregulation of calpain activity precedes tau phosphorylation and loss of synaptic proteins in Alzheimer's disease brain. *Acta Neuropathol Commun*. 2016;4:34.
66. Ballatore C, Lee VM, Trojanowski JQ. Tau-mediated neurodegeneration in Alzheimer's disease and related disorders. *Nat Rev Neurosci*. 2007;8:663-672.
67. Carlyle BC, Nairn AC, Wang M. cAMP-PKA phosphorylation of tau confers risk for degeneration in aging association cortex. *Proc Natl Acad Sci USA*. 2014;111:5036-5041.
68. Thal DR, Del Tredici K, Ludolph AC, et al. Stages of granulovacuolar degeneration: their relation to Alzheimer's disease and chronic stress response. *Acta Neuropathol*. 2011;122:577-589.
69. Rauch JN, Luna G, Guzman E, et al. LRP1 is a master regulator of tau uptake and spread. *Nature*. 2020;580:381-385.
70. Calafate S, Flavin W, Verstreken P, Moechars D. Loss of bin1 promotes the propagation of tau pathology. *Cell Rep*. 2016;17:931-940.
71. Rissman RA, Langford O, Raman R, et al. Plasma Abeta42/Abeta40 and phospho-tau217 concentration ratios increase the accuracy of amyloid PET classification in preclinical Alzheimer's disease. *Alzheimers Dement*. 2023. <https://pubmed.ncbi.nlm.nih.gov/37932961/>
72. Yamashima T. Reconsider Alzheimer's disease by the 'calpain-cathepsin hypothesis'-a perspective review. *Prog Neurobiol*. 2013;105:1-23.
73. Moloney CM, Lowe VJ, Murray ME. Visualization of neurofibrillary tangle maturity in Alzheimer's disease: a clinicopathologic perspective for biomarker research. *Alzheimers Dement*. 2021;17:1554-1574.
74. Rajbanshi B, Guruacharya A, Mandell JW, Bloom GS. Localization, induction, and cellular effects of tau phosphorylated at threonine 217. *Alzheimers Dement*. 2023;19:2874-2887.
75. Choy RW, Cheng Z, Schekman R. Amyloid precursor protein (APP) traffics from the cell surface via endosomes for amyloid beta (Abeta) production in the trans-Golgi network. *P Natl Acad Sci USA*. 2012;109:E2077-E2082.
76. Barthelemy NR, Saef B, Li Y, et al. CSF tau phosphorylation occupancies at T217 and T205 represent improved biomarkers of amyloid and tau pathology in Alzheimer's disease. *Nat Aging*. 2023;3:391-401.



77. Dai CL, Chen X, Kazim SF, et al. Passive immunization targeting the N-terminal projection domain of tau decreases tau pathology and improves cognition in a transgenic mouse model of Alzheimer disease and tauopathies. *J Neural Transm (Vienna)*. 2015;122:607-617.
78. Dai CL, Tung YC, Liu F, Gong CX, Iqbal K. Tau passive immunization inhibits not only tau but also Abeta pathology. *Alzheimers Res Ther*. 2017;9:1.

#### SUPPORTING INFORMATION

Additional supporting information can be found online in the Supporting Information section at the end of this article.

**How to cite this article:** Datta D, Perone I, Wijegunawardana D, et al. Nanoscale imaging of pT217-tau in aged rhesus macaque entorhinal and dorsolateral prefrontal cortex: Evidence of interneuronal trafficking and early-stage neurodegeneration. *Alzheimer's Dement*. 2024;20:2843-2860. <https://doi.org/10.1002/alz.13737>